Cell Stem Cell
Article

Genome-wide Maps of Histone Modifications Unwind In Vivo Chromatin States of the Hair Follicle Lineage

Wen-Hui Lien,[1] Xingyi Guo,[2] Lisa Polak,[1] Lee N. Lawton,[5] Richard A. Young,[5,6] Deyou Zheng,[2,3,4] and Elaine Fuchs[1,*]
[1]Howard Hughes Medical Institute, Laboratory of Mammalian Cell Biology & Development, The Rockefeller University, New York, NY 10065, USA
[2]Department of Neurology
[3]Department of Genetics
[4]Department of Neuroscience
Albert Einstein College of Medicine, Bronx, NY 10461, USA
[5]Whitehead Institute for Biomedical Research, Cambridge, MA 02139, USA
[6]Department of Biology, Massachusetts Institute of Technology, Cambridge, MA 02139, USA
*Correspondence: fuchslb@rockefeller.edu
DOI 10.1016/j.stem.2011.07.015

SUMMARY

Using mouse skin, where bountiful reservoirs of synchronized hair follicle stem cells (HF-SCs) fuel cycles of regeneration, we explore how adult SCs remodel chromatin in response to activating cues. By profiling global mRNA and chromatin changes in quiescent and activated HF-SCs and their committed, transit-amplifying (TA) progeny, we show that polycomb-group (PcG)-mediated H3K27-trimethylation features prominently in HF-lineage progression by mechanisms distinct from embryonic-SCs. In HF-SCs, PcG represses nonskin lineages and HF differentiation. In TA progeny, nonskin regulators remain PcG-repressed, HF-SC regulators acquire H3K27me3-marks, and HF-lineage regulators lose them. Interestingly, genes poised in embryonic stem cells, active in HF-SCs, and PcG-repressed in TA progeny encode not only key transcription factors, but also signaling regulators. We document their importance in balancing HF-SC quiescence, underscoring the power of chromatin mapping in dissecting SC behavior. Our findings explain how HF-SCs cycle through quiescent and activated states without losing stemness and define roles for PcG-mediated repression in governing a fate switch irreversibly.

INTRODUCTION

Most mammals rely on hair for warmth and protection. HFs undergo synchronized, cycles of growth (anagen), destruction (catagen), and rest (telogen). Cyclical regeneration and hair growth is fueled by stem cells (SCs) residing in a region of the follicle outer root sheath (ORS) known as the bulge (Blanpain and Fuchs, 2009; Cotsarelis et al., 1990). During telogen, the bulge niche resides at the HF base, in association with a mesenchymal stimulus, called the dermal papilla (DP). Despite close proximity of DP during telogen, HF-SCs remain quiescent because of extrinsic inhibitory signals within the niche (Hsu et al., 2011). As activating cues by DP and other niche cells accumulate toward the end of telogen, HF-SCs begin to proliferate. Soon thereafter, a new HF emerges.

As the HF matures and grows downward, the DP moves progressively away from the HF-SC niche. By mid-anagen, HF-SCs return to quiescence. The transient-amplifying matrix cells (TACs) maintain contact with the DP stimulus at the HF base and continue to proliferate. HF-TACs undergo several rapid divisions and then terminally differentiate to generate the seven lineages of hair and its channel (Blanpain and Fuchs, 2009; Hsu et al., 2011). This spatially and temporally well-defined program makes the HF an excellent model for studying how SCs transition reversibly from quiescent to active states and how their properties change irreversibly as they become TAC progeny fated to differentiate.

Quiescent HF-SCs preferentially express surface markers CD34, Lgr5, $\alpha6\beta4$, and $\alpha3\beta1$ integrins, as well as transcription factors (TFs) Lhx2, Sox9, Nfatc1, Tcf3, and Tcf4 (Blanpain and Fuchs, 2009). Their activation depends upon HF-SC:DP cross-talk involving BMP inhibitory and Wnt activating factors, resulting in lineage progression (Greco et al., 2009). Little is known about the extent to which these changes occur at the transcriptional level or how epigenetic mechanisms impact HF-SC behavior and lineage determination.

Increasing evidence suggests that specific histone modifications are associated with actively transcribed protein-coding genes. Initiated genes are marked near their transcription start sites (TSSs) by nucleosomes whose histone H3 subunits are trimethylated on lysine 4 (H3K4me3). Additional histone modifications, including histone H3 lysine 79 dimethylation (H3K79me2) and H3 lysine 36 trimethylation (H3K36me3), occur within the body of the gene, as RNA polymerase II progresses through chromatin (Li et al., 2007; Pokholok et al., 2005; Vakoc et al., 2006). Strongly transcribed genes are often associated with an additional broadening of the H3K4me3 peak (Adli et al., 2010; Mikkelsen et al., 2007).

Although these modifications reflect the nuts and bolts of the transcription state, transcription is a continuum of silenced, paused, and active states that are indicated by additional chromatin modifications. In this regard, the polycomb group (PcG) modification, H3 lysine 27 trimethylation (H3K27me3) of histone

tails, is particularly important. PcG complexes occupy and silence genes encoding lineage-restricted developmental regulators. In cultured embryonic stem cells (ESCs), PcG-repression contributes to maintaining pluripotency (Kirmizis et al., 2004; Bernstein et al., 2006; Mikkelsen et al., 2007; Barski et al., 2007; Zhao et al., 2007). Interestingly, key developmental genes exist in a "bivalent" or "poised" state in ESCs and display both the PcG-repressive H3K27me3 mark and the H3K4me3 mark of initiation (Bernstein et al., 2006). Many of these genes are resolved to either active or repressed states when ESCs are differentiated in vitro to become neural progenitors and fibroblasts (Mikkelsen et al., 2007).

Although genome-wide chromatin mapping has provided new insights into cellular states that go beyond mRNA expression profiling, it is not yet clear whether such mechanisms are physiologically relevant or how they may play out in adult SCs, such as HF-SCs, in which there are multiple steps in lineage commitment. Genetic analyses suggest a role for H3K27 methyltransferases Ezh1 and/or Ezh2 in morphogenesis and maintenance of embryonic/neonatal tissues, including epidermis and HFs (Chen et al., 2009; Ezhkova et al., 2011; Ezhkova et al., 2009; Su et al., 2003). PcG loss of function seems to specifically affect SC self-renewal, which has been attributed to derepression of cell cycle inhibitor genes within the *Ink4a/Ink4b/Arf* locus. Although these findings expose the sensitivity of this locus to loss of H3K27me3, these genes are normally silent in most adult tissues. Moreover, the potent consequences of aberrant activation of the locus have precluded explorations into how PcG repression governs SC lineage determination in a normal context.

We now investigate this important question in the HF, which is among the few adult tissues in which SCs and their TA progeny can be purified in sufficient quantities to conduct chromatin immunoprecipitation and deep sequencing (ChIP-seq). By conducting ChIP-seq and mRNA profiling on cells in their native state, we have uncovered global chromatin modifications that occur as a quiescent adult SC transitions first through an activated state and then to a committed state along its lineage. We show that in contrast to ESCs, very few bivalent H3K27me3+H3K4me3 genes are found within HF-SCs, similar to neural precursors differentiated from ESCs in vitro. Moreover, by classifying genes that are (1) bivalent in ESCs, (2) active in quiescent and/or proliferating HF-SCs, and (3) PcG-silenced in HF-TACs, we unveil a short list of genes that are dramatically enriched for known master regulators of HF-SCs. Similarly, by defining genes that are (1) PcG-repressed in HF-SCs and (2) active in HF-TACs, we unearth a short list enriched for master regulators of matrix. These findings suggest that these lists are enriched for other key regulators, as yet unstudied. We test this hypothesis on several signaling factors that appeared unexpectedly on these lists. By coupling the transcriptional status of their corresponding receptors with functional studies on the ligands, we demonstrate the biological value of mapping chromatin states in vivo. Taken together, our studies reveal a potent PcG switch that is not triggered when HF-SCs transition from a quiescent to active state, but rather functions both to silence key regulators of HF-SC and release regulators of committed matrix cells. Our data suggest that PcG-mediated regulation places a molecular threshold on the irreversible transition from a multipotent activated SC to a differentiation-committed TA cell. These new findings illuminate how HF-SCs might induce self-renewal while retaining their "stemness" as they receive activating signals at the start of the hair cycle.

RESULTS

Purifying Quiescent and Activated SCs and Their TA Progeny from Adult HFs

For determining the possible physiological relevance of chromatin modifications to the program of gene expression in adult SCs and their lineages, our aim was to map mRNA expression profiles and global chromatin occupancies of key histone modifications in HFs in their native context. The technological demands of ChIP-seq were met by the synchrony of HFs, enabling us to purify 10^7 cells of each of three desired populations for our study: quiescent HF-SCs (qHF-SCs), activated HF-SCs (aHF-SCs), and TA-matrix cells (HF-TACs) (Figure 1A).

For each experiment, we used fluorescence activated cell sorting (FACS) and ~10–15 adult female CD-1 mice transgenic for *K14-GFP*, active in skin epithelium (Rendl et al., 2005). qHF-SCs were isolated from telogen HFs in the midst (postnatal day P52–58) of a 3 week resting phase. Whereas the aHF-SC population will always contain quiescent SCs, appreciable SC cycling exists in the early-mid growth phase (anagen) (Hsu et al., 2011). Hence, we chose P28–30 for isolating aHF-SCs and HF-TACs. Populations were sorted on the basis of GFP fluorescence and Abs against differentially expressed surface proteins (Figure 1B). In addition to established markers of bulge HF-SCs (CD34, α6 integrin; Blanpain et al., 2004), Sca1-Abs were used for removing/discarding basal epidermal and upper ORS cells and ephrin B1-Abs enriched for HF-TACs. Immunofluorescence of cytospin samples confirmed >95% purity for each population.

Molecular Signatures of HF Lineage States

Total RNAs from each population were analyzed in duplicate by microarray for expression of ~30,000 mouse genes. Comparisons provided molecular signatures of mRNAs $\geq$ 2X increased in one population relative to the others ($p < 0.02$). The signatures are presented as a heat map (Figure 1C) and were confirmed by reverse transcription (RT) and quantitative (q)-PCR (Figure S1 available online).

As expected from previous studies (Lowry et al., 2005), mRNAs expressed by aHF-SCs and qHF-SCs overlapped significantly (n = 672) and included key HF-SC TFs (Figure S1A). In addition, genes involved in cell signaling appeared on this list (Figure 1D; Table S1). The qHF-SC-specific signature (n = 651) was enriched for balancers of cell survival/apoptosis and negative regulators of gene expression ($p < 0.001$). The aHF-SC signature (n = 231, anagen bulge alone) favored mRNAs associated with cell migration/proliferation ($p < 0.001$) (Figure 1D; Table S1). The HF-TAC signature was the most highly enriched for cell cycle enhancing as well as HF lineage/differentiation mRNAs, e.g., *Lef1*, *Msx1*, and *Cux1* (Figure S1B; Table S1; $p < 0.001$). These new comparisons provided a more comprehensive and clearer picture than previously of the changes in mRNA expression that occur as HF-SCs transition from a quiescent to activated and finally TA state. Importantly, they also established

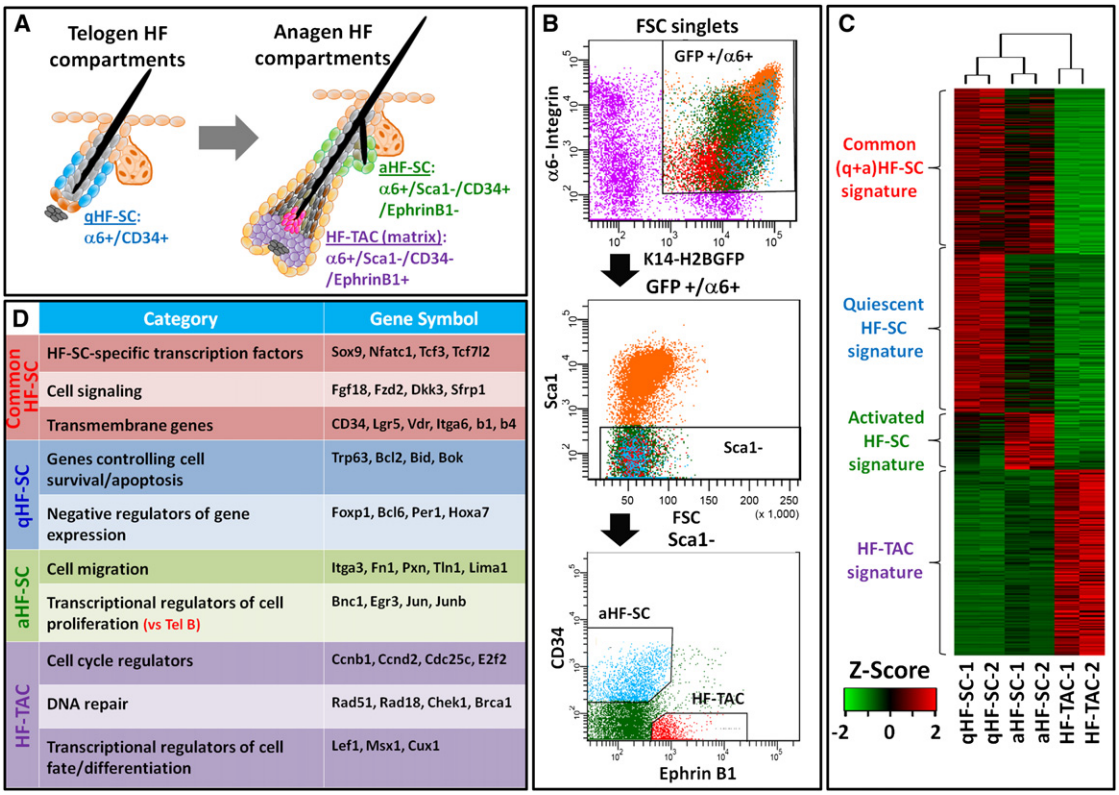

D

	Category	Gene Symbol
Common HF-SC	HF-SC-specific transcription factors	Sox9, Nfatc1, Tcf3, Tcf7l2
	Cell signaling	Fgf18, Fzd2, Dkk3, Sfrp1
	Transmembrane genes	CD34, Lgr5, Vdr, Itga6, b1, b4
qHF-SC	Genes controlling cell survival/apoptosis	Trp63, Bcl2, Bid, Bok
	Negative regulators of gene expression	Foxp1, Bcl6, Per1, Hoxa7
aHF-SC	Cell migration	Itga3, Fn1, Pxn, Tln1, Lima1
	Transcriptional regulators of cell proliferation (vs Tel B)	Bnc1, Egr3, Jun, Junb
HF-TAC	Cell cycle regulators	Ccnb1, Ccnd2, Cdc25c, E2f2
	DNA repair	Rad51, Rad18, Chek1, Brca1
	Transcriptional regulators of cell fate/differentiation	Lef1, Msx1, Cux1

Figure 1. Molecular Signatures of mRNAs for Quiescent and Activated States of SCs and Their TA Progeny in Adult HFs

(A) Schematic of adult HF compartments and cell surface markers used for FACS.

(B) Sequential FACS purifications of aHF-SCs and HF-TACs from anagen HFs. Purifications of qHF-SCs were as described (Blanpain et al., 2004).

(C) Heat map and clustering of mRNA expression profiles of signature genes.

(D) Functional categories of gene ontology and representative examples of mRNAs upregulated ≥2× in (1) quiescent, active or common HF-SCs relative to HF-TAC; and (2) HF-TAC relative to HF-SCs. Signatures in (C) and (D) are according to cell populations in (A). See also Figure S1 and Table S1.

steady state expression profiles for each population to subsequently compare to their chromatin states.

Genome-wide Profiles of H3K4me3 and H3K27me3 Unveil Differences between qHF-SCs and ESCs

In cultured ESCs, genes encoding key master regulators of lineages are bivalent/poised, i.e., marked by both H3K4me3 and by H3K27me3; in embryonic fibroblasts (MEFs), these genes are partially resolved; in neural progenitor cells (NPCs), they are largely resolved to either a fully repressed or fully activated state (Figure 2A; Lee et al., 2006; Mikkelsen et al., 2007). Given these in vitro findings and the potential importance of PcG modifications to adult SCs in vivo, we used ChIP-seq to determine the global progenitor H3K4me3 and H3K27me3 modification profiles from our purified skin populations.

Ninety percent of H3K4me3 peaks identified in qHF-SCs were located within ±2 kb of promoter regions of known genes/transcripts (Table S2). Moreover, similar to in vitro lineage-committed progenitors and in striking contrast to ESCs, qHF-SCs in vivo displayed very few genes (89/15,284) in a bivalent state (Figure 2A). These results added in vivo relevance to the prior notion that the bivalent, "poised" state may be uniquely tailored to enable ESCs to maintain the flexibility to choose among a myriad of lineage options (Bernstein et al., 2006; Boyer et al., 2006; Lee et al., 2006; Mikkelsen et al., 2007).

The majority of promoters bivalent in ESCs were resolved to either H3K4me3 alone (39%) or H3K27me3 (38%) in qHF-SCs (Figure 2B). Interestingly, genes bivalent in ESCs but PcG-repressed in qHF-SCs included not only key genes in nonskin tissue-specific lineages but also hair lineage differentiation (Figure 2C; Table S3). In contrast to bivalent genes, most ESC genes marked only by H3K4me3 were similarly marked in qHF-SCs (Figure 2B). Predictably, ChIP-seq showed that RNA polymerase II also marked most of these genes (data not shown). Because the majority of these singly marked genes were also activated in MEFs and NPCs, this list seemed to be enriched for features (including housekeeping functions) common to progenitor states and irrespective of cycling status.

Only 2.3% of genes marked by only H3K4me3 in ESCs were transcriptionally repressed by H3K27me3 in qHF-SCs (Figure 2B). That said, this short list was informative, as exemplified by its inclusion of *Sox2* (Figure 2D), which, along with Oct4, Nanog, and Tcf3, establishes the genomic state that maintains ESC pluripotency (Bernstein et al., 2006; Boyer et al., 2005; Boyer et al., 2006; Lee et al., 2006). Only Tcf3, a transcriptional effector

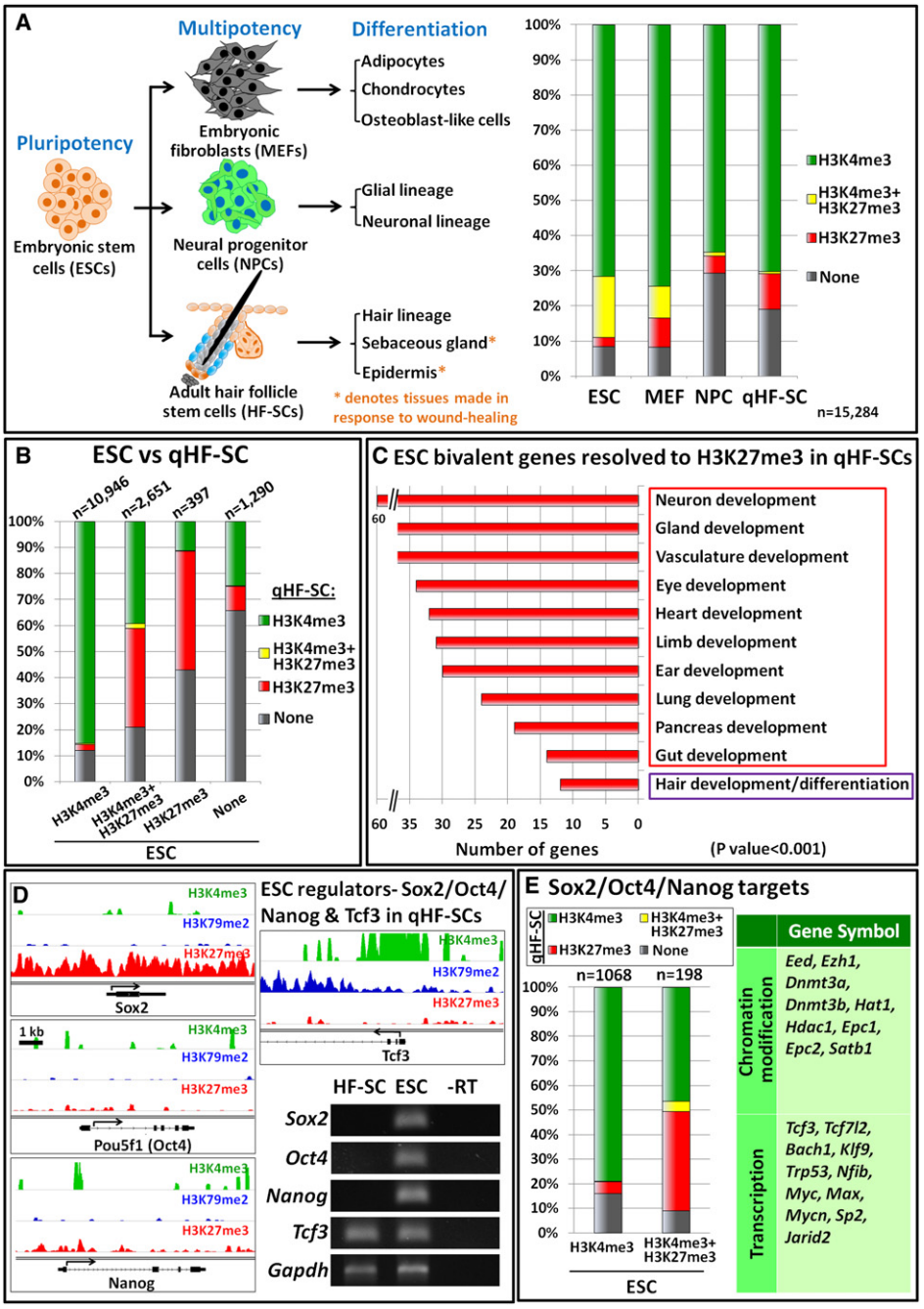

Figure 2. Genome-wide Mapping of H3K4me3 and H3K27me3 Profiles in qHF-SCs

(A) Global in vivo H3K4me3 and H3K27me3 patterns in qHF-SC chromatin, compared with published in vitro data on chromatin from cultured murine ESCs, MEFs and NPCs (Mikkelsen et al., 2007). In contrast to ESCs and MEFs, very few bivalent genes (yellow) were detected in qHF-SCs or NPCs.

(B) Genes that in ESCs displayed one of four H3 methylation patterns (horizontal axis) and how this changes in qHF-SC chromatin. Each bar is normalized to 100% (n = number of ESC genes with each mark). Color coding is for the qHF-SC genes and denotes the percentage of total genes within the ESC gene set that has either the same or a different mark in qHF-SCs. Green, H3K4me3; yellow, bivalent/dual marked with H3K4me3 and H3K27me3; red, H3K27me3; gray, neither mark. Note that most genes that were bivalent in ESCs are either H3K4me3 (primed/active) or H3K27me3 (repressed) in qHF-SCs.

(C) Gene ontologies of bivalent ESC genes that display only H3K27me3 in qHF-SCs. Ontology terms are shown on the y axis; numbers of genes that fall into each category based upon functional studies are graphed along the x axis.

(D) Except for *Tcf3*, ESC pluripotency genes are not transcribed in qHF-SCs. Shown are ChIP-seq signal tracks across indicated genes. Exon-intron structures and coding strand direction are depicted beneath. All tracks are set to the same scale (0–50); IGV browser. RT-PCR: pluripotency mRNAs from qHF-SCs and ESCs. Negative (−RT) and positive (*Gapdh*) controls.

(E) Despite the silencing of pluripotency genes in qHF-SCs, ~80% of Sox2/Oct4/Nanog direct targets that are H3K4me3+ in ESCs (Boyer et al., 2006; Cole et al., 2008) are also H3K4me3+ in qHF-SCs. Examples of these genes are listed in the table. See also Table S2 and Table S3.

of Wnt signaling that intersects with the ESC core circuitry (Cole et al., 2008), was also actively transcribed in HF-SCs and also critical for their maintenance (Figure 2D; Nguyen et al., 2009).

Surprisingly, despite the silenced state of pluripotency genes in HF-SCs, only a small subset of the genes bound by Sox2/Oct4/Nanog and H3K4me3-marked in ESCs (Cole et al., 2008; Marson et al., 2008) were PcG repressed in qHF-SCs (Figure 2E). Most, including Tcf3 and many other chromatin regulators, were active in both SC types. Conversely, of the HF-SC signature genes, >60% also scored as active in ESCs, including cell cycle regulation and apoptosis/survival genes (data not shown). Together, these data suggest that a common set of chromatin, transcriptional, and cell cycle/survival regulators may govern both pluripotent, rapidly proliferating ESCs and lineage-restricted, slow-cycling HF-SCs. Moreover, since *Sox2*, *Oct4*, and *Nanog* are not expressed by HF-SCs, other TFs must contribute to the activation of these core stemness target genes in adult SCs.

Identifying Key HF Regulators from Aspects of Histone Modification

Because bivalent ESC genes include developmental regulators required for lineage specification, it seemed likely that key regulators of HF-SC specification and maintenance might be bivalent in ESC and H3K4me3-marked genes in qHF-SCs. Consistent with this notion, TF family genes that were bivalent in ESCs and PcG-derepressed in qHF-SCs were often featured in the HF-SC signature (Figure 3A; Table S4A). This included *Sox9*, *Lhx2*, *Gata3*, *Runx1*, *Dlx3* and *Hoxc13*, whose functional importance to the hair lineage is known (Fuchs, 2007) (Figure 3B; Table S4B). The significant enrichment of established regulators led us to wonder whether less explored members of this list, e.g., TF genes *Foxc1*, *Klf4*, *Irx*, and *Tbx1*, or signaling factor genes, e.g., *Fgf18*, *Grem1*, *Fst*, and *Inhbb*, might also play critical roles in HF-SC behavior.

In ESCs, key pluripotency genes such as *Oct4* (*Pouf5f1*) display expanded H3K4me3 peaks over their promoters (Mikkelsen et al., 2007), and in hematopoietic progenitors, broad H3K4me3 domains coincide with known hematopoietic regulators (Adli et al., 2010). To address whether similar features might be characteristic of key HF-SC regulators, we analyzed H3K4me3 peak sizes in the promoter regions of qHF-SC genes. One hundred eighty qHF-SC genes displayed expanded peaks (>4 kb) and were highly enriched for HF-SC signature genes (47% versus 10%; $p < 0.001$). Genes encoding HF-SC marker proteins, e.g., CD34 and K15, were included in this group, as were essential HF-SC TF genes *Lhx2*, *NFATc1*, and *Sox9* (Figure 3C). The sheer number of TFs (32; 38%) in this group was notable, given that only 10% of all mouse genes encode TFs. Curiously, many of the same signaling factors noted above also appeared on this list.

Transitioning to HF-TACs Involves PcG-Mediated Repression of HF-SC Genes

To determine whether and how epigenetic changes might be involved in the HF lineage, we developed genome-wide maps of histone modifications for quiescent versus activated HF-SCs and for HF-TACs. For this study, we included H3K79me2, which distinguishes initiated (H3K4me3 only) from actively elongating (H3K4me3+H3K79me2) transcripts (Vakoc et al., 2006). As expected, promoters of genes marked by H3K79me2 in our populations were always modified by H3K4me3 as well (Figure 4A). Conversely, ~20%–30% displayed only the H3K4me3 mark and not the H3K79me2, even when analyses were restricted to genes preferentially transcribed in these populations (Figure 4B).

By comparing chromatin and mRNA expression data, we learned that genes displaying the H3K79me2 mark were on average transcribed at higher levels than those with only the H3K4me3 mark (Figure 4B, Figure S2A). This analogy seemed to be meaningful, given that 31% of H3K4me3-marked genes in HF-SCs gained the H3K79me2 mark in HF-TACs (Figure 4C), and these genes were more highly expressed than those retaining solely the H3K4me3-mark in HF-TACs ($p < 0.001$; Figure S2B). These data suggested that the acquisition of an H3K79me2 mark can provide an epigenetic readout to gauge transcriptional levels within a lineage.

Among qHF-SC signature genes marked by H3K4me3 ± H3K79me2, only 12.5% became PcG silenced in HF-TACs (Figure 4B). Intriguingly, 66.5% of this subset exists in a bivalent repressed state in ESCs. Underscoring the potential importance of this group was the inclusion of established HF-SC genes e.g., *CD34*, *Sox9*, *Nfatc1*, and *Fgf18.* Intriguingly, the putative cell signaling regulators, *Grem1*, *Fst*, and *Gdf10*, surfaced again on this list (Figure 4D; Table S5).

The importance of PcG-mediated chromatin modifications in repressing SC regulators upon HF-TAC commitment was further highlighted by comparing histone modification peak intensities on key PcG-regulated HF-SC genes versus housekeeping genes expressed in both SCs and TACs. As shown in Figure 4E, key HF-SC signature genes were enriched for H3K4me3 and H3K79me2 modifications in HF-SCs, but showed H3K27me3 repression in HF-TACs.

HF-TAC Commitment Involves Derepression of PcG-Silenced Key Matrix Regulators

Before terminally differentiating along one of seven different HF lineages, matrix cells undergo a brief spurt of proliferation as undifferentiated cells. During this time, HF-SC regulators are repressed while a unique set of matrix regulators are induced (Blanpain and Fuchs, 2009). To determine whether the matrix induction switch is also governed by PcG, we compared the chromatin state of HF-TAC signature genes in matrix where they are active to the bulge where they are silenced.

Seventy-seven percent of HF-TAC signature genes displayed H3K4me3 and H3K79me2 modifications, reflective of a highly transcribed state (Figure 5A). Many of these genes were "induced" (acquired H3K79me2 mark; n = 312) during the qHF-SC to TAC switch, whereas only a small subset were "derepressed" (lost H3K27me3 mark; n = 18) from a PcG-repressed state (Table S6). Bioinformatics analyses revealed that the "induced" TAC subset was composed mostly of cell cycle-related genes, whereas the "derepressed" PcG group encompassed known regulators of matrix biology (e.g., *Lef1*, *Cux1*, *Sp6*, *Runx2*, and *Msx1*) (Figure 5B).

Peak intensities of histone modifications further highlighted the dynamic chromatin states of HF-TACs (Figure 5C). Consistent with the markedly enhanced proliferation in HF-TACs, cell

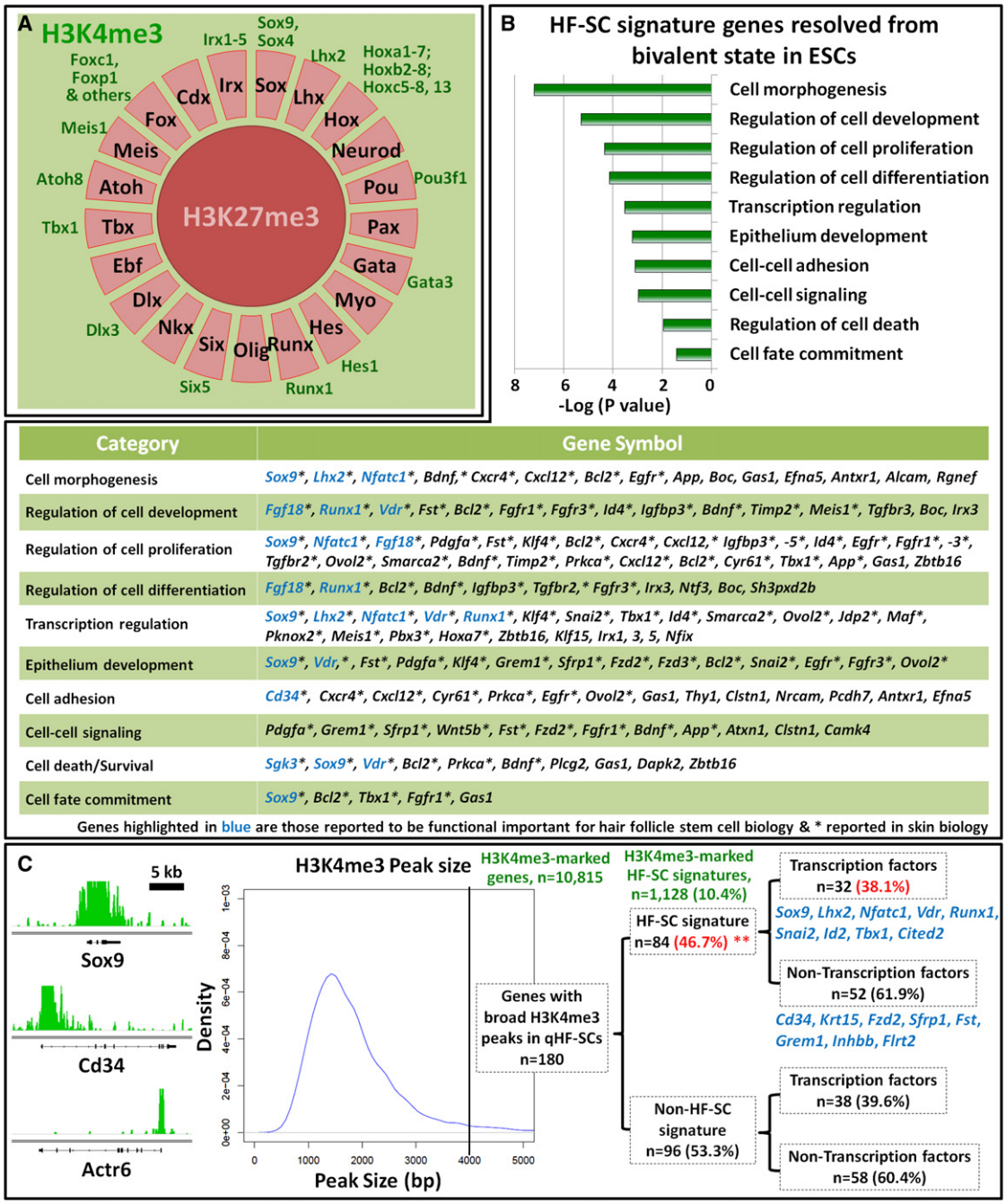

Category	Gene Symbol
Cell morphogenesis	*Sox9*, Lhx2*, Nfatc1*, Bdnf,* Cxcr4*, Cxcl12*, Bcl2*, Egfr*, App, Boc, Gas1, Efna5, Antxr1, Alcam, Rgnef*
Regulation of cell development	*Fgf18*, Runx1*, Vdr*, Fst*, Bcl2*, Fgfr1*, Fgfr3*, Id4*, Igfbp3*, Bdnf*, Timp2*, Meis1*, Tgfbr3, Boc, Irx3*
Regulation of cell proliferation	*Sox9*, Nfatc1*, Fgf18*, Pdgfa*, Fst*, Klf4*, Bcl2*, Cxcr4*, Cxcl12,* Igfbp3*, -5*, Id4*, Egfr*, Fgfr1*, -3*, Tgfbr2*, Ovol2*, Smarca2*, Bdnf*, Timp2*, Prkca*, Cxcl12*, Bcl2*, Cyr61*, Tbx1*, App*, Gas1, Zbtb16*
Regulation of cell differentiation	*Fgf18*, Runx1*, Bcl2*, Bdnf*, Igfbp3*, Tgfbr2,* Fgfr3*, Irx3, Ntf3, Boc, Sh3pxd2b*
Transcription regulation	*Sox9*, Lhx2*, Nfatc1*, Vdr*, Runx1*, Klf4*, Snai2*, Tbx1*, Id4*, Smarca2*, Ovol2*, Jdp2*, Maf*, Pknox2*, Meis1*, Pbx3*, Hoxa7*, Zbtb16, Klf15, Irx1, 3, 5, Nfix*
Epithelium development	*Sox9*, Vdr,* , Fst*, Pdgfa*, Klf4*, Grem1*, Sfrp1*, Fzd2*, Fzd3*, Bcl2*, Snai2*, Egfr*, Fgfr3*, Ovol2**
Cell adhesion	*Cd34*, Cxcr4*, Cxcl12*, Cyr61*, Prkca*, Egfr*, Ovol2*, Gas1, Thy1, Clstn1, Nrcam, Pcdh7, Antxr1, Efna5*
Cell-cell signaling	*Pdgfa*, Grem1*, Sfrp1*, Wnt5b*, Fst*, Fzd2*, Fgfr1*, Bdnf*, App*, Atxn1, Clstn1, Camk4*
Cell death/Survival	*Sgk3*, Sox9*, Vdr*, Bcl2*, Prkca*, Bdnf*, Plcg2, Gas1, Dapk2, Zbtb16*
Cell fate commitment	*Sox9*, Bcl2*, Tbx1*, Fgfr1*, Gas1*

Genes highlighted in blue are those reported to be functional important for hair follicle stem cell biology & * reported in skin biology

Figure 3. Identifying Key HF Regulators from Aspects of Histone Modification

(A) Classifications of mouse transcription factor (TF) genes that are bivalent or PcG-repressed in ESCs and their chromatin status in qHF-SCs. Most genes within each superfamily are repressed (red) in qHF-SCs. Of the small number of these genes that are active (green), ~50% are known to be functionally important in HF-SCs.

(B) Classifications and associated examples of lineage-specific HF-SC signature genes (H3K4me3+) that exist in a bivalent state in ESCs. Highlighted are genes previously implicated in skin biology in general (*) or HF-SCs in particular (blue).

(C) Examples of HF-SC signature genes (*Sox9*, *Cd34*) displaying broad H3K4me3 peaks in qHF-SCs compared to a housekeeping gene (*Actr6*). Shown at right are peak size distributions of H3K4me3 intervals associated with all promoters marked by H3K4me3 in qHF-SCs. Of the genes with broad (>4 kb) peaks, 46.7% are in the HF-SC signature, compared to only 10.4% among all H3K4me3-marked genes (**$p < 0.001$; examples in blue). Note that TFs with broad H3K4me3 peaks are highly enriched in both nonsignature and signatures. See also Table S4.

cycle genes were transcribed at much higher levels than in qHF-SCs (compare intensities of H3K79me2 marks). However, the most striking chromatin differences occurring as HF-SCs transitioned to HF-TACs were in H3K27me3 marks, where key matrix genes were PcG-derepressed, and key HF-SC genes were repressed.

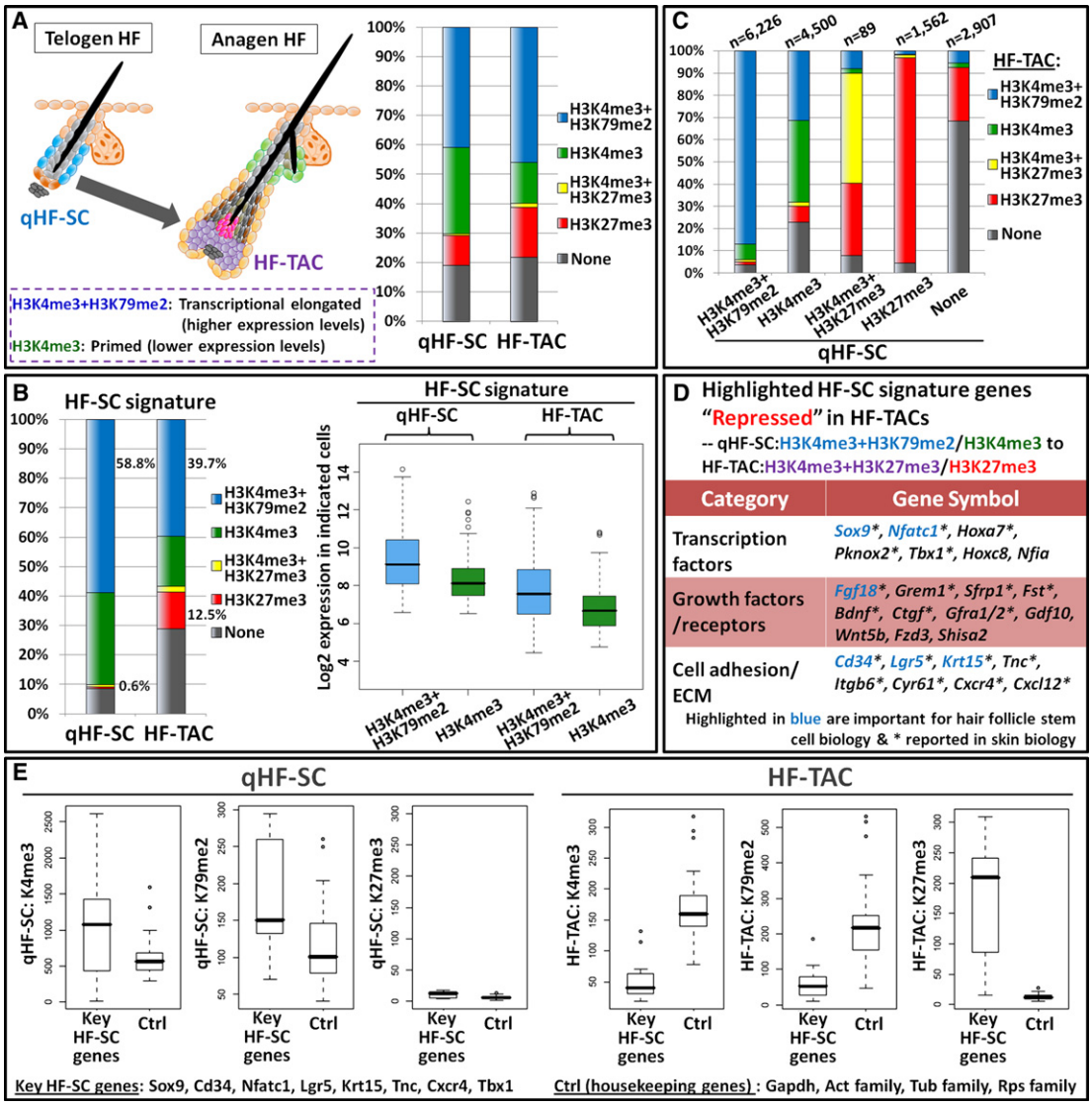

Figure 4. The Transition from HF-SCs to HF-TACs Involves PcG-Mediated Gene Repression of Key Stemness Genes

(A) Schematic of the two cell populations used for the comparisons described in this figure. On the right are global histone methylation patterns of chromatin from qHF-SCs and matrix HF-TACs. Note paucity of H3K4me3+H3K27me3 marked genes (yellow bar).

(B) As shown on the left, 12.5% of HF-SC signature genes are PcG-repressed in HF-TACs (red). As shown on the right, mRNA expression (Log2) of HF-SC signature genes marked by H3K4me3+H3K79me2 is much greater in qHF-SCs than equivalently marked genes in HF-TACs. H3K4me3+H3K79me2 marked genes (blue) are more highly expressed than genes marked only by H3K4me3 (green).

(C) How H3 methylation patterns of qHF-SC chromatin change during the transition to HF-TACs. Genes (total numbers indicated above each bar) displaying a particular chromatin state in qHF-SCs (indicated below each bar) were analyzed for their H3 methylation patterns in HF-TACs (color coded as indicated). Note that only a small number of genes repressed or bivalent in qHF-SCs are now active in HF-TACs. Note also that some genes marked by H3K4me3 in qHF-SCs are now H3K27me3-repressed in HF-TACs.

(D) Gene ontologies and associated examples of HF-SC signature genes that go from an active to repressed state in HF-TACs. Note that key HF-SC TF genes are among this shortlist.

(E) Box and whisker plots of H3K4me3 and H3K79me2 peak intensities over key HF-SC genes versus housekeeping/control genes (examples provided beneath the plots) as analyzed both in qHF-SCs and in HF-TACs. Note that peak intensities are greatest for key genes in qHF-SCs and that marked reductions in these chromatin marks occur upon transition to the TA state. See also Figure S2 and Table S5.

Maintaining Stemness during the Transition from a Quiescent to Proliferative State: Inducing Cell Cycle Regulators without Affecting Key PcG-regulated Matrix Genes

In striking contrast to HF-TACs, genes expressed by aHF-SCs retained many of the same modifications and displayed similar mRNA patterns as their quiescent counterparts (Figures 6A and 1). Notably, aHF-SCs showed no signs of the PcG-silencing of key HF-SC genes that occurred in HF-TACs (e.g., *Sox9* in Figure 6B). Interestingly, although only 3.3% of HF-SC signature genes acquired PcG-repressive marks in aHF-SCs (Figure 6A), this small group included genes that encode known regulators

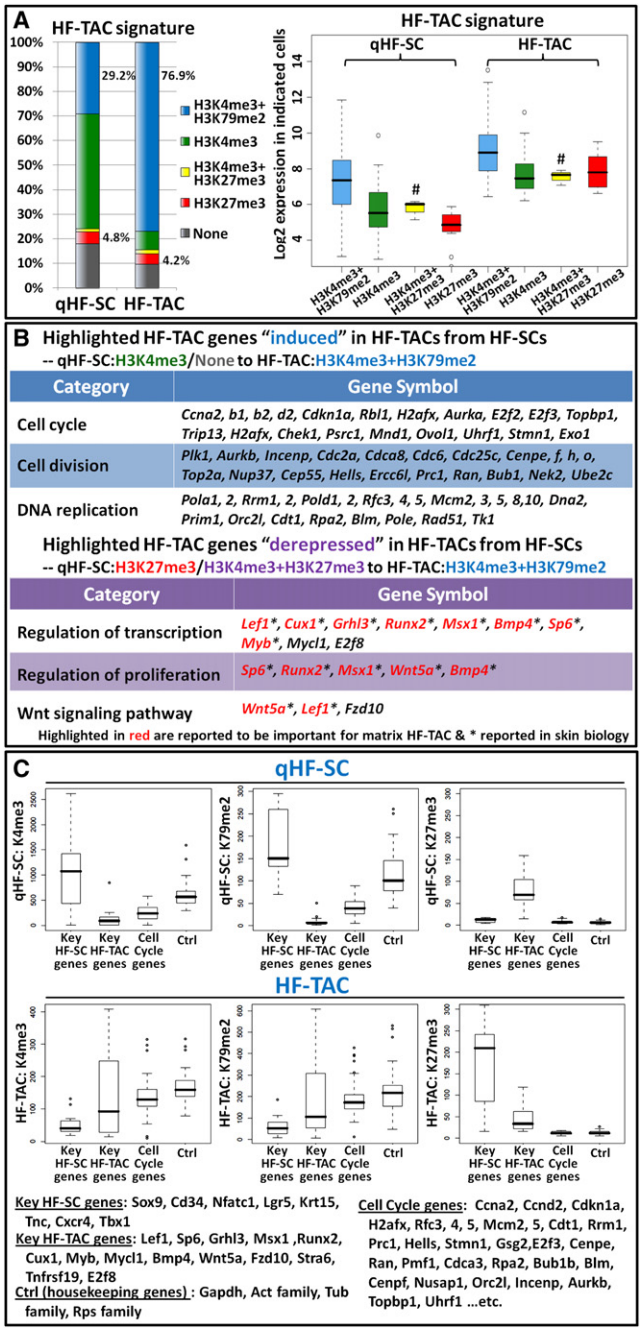

Figure 5. Transitioning from HF-SCs to HF-TACs Involves PcG-Mediated Gene Derepression of Key HF-TAC Regulators

(A) Many HF-TAC signature genes show H3K4me3+ marks in qHF-SCs but H3K4me3+H3K79me2 marks in HF-TACs. At right are HF-TAC signature mRNA levels (Log2) of genes that display the indicated chromatin states in qHF-SCs versus HF-TACs. Note that HF-TAC signature mRNAs are always higher in HF-TACs versus HF-SCs, irrespective of which chromatin mark is compared. #, n = 3.

(B) In the HF-SC→HF-TAC switch, "induced" HF-TAC signature genes are largely cell cycle genes (blue), whereas "derepressed" HF-TAC signature genes are mostly known key matrix regulators (purple). Genes known to be important for skin biology (*) or for matrix HF-TAC function (red) are highlighted.

(C) Box and whisker plots to show H3 modification peak intensities over signature genes for qHF-SCs (top) or HF-TACs (bottom) that fall into one of the four categories indicated (representative genes provided below the plots). Note that key matrix regulators display strong repressive peak intensities in qHF-SCs. This repression is then relieved in HF-TACs accompanied by increased intensities of H3K4me3 and H3K79me3 peaks. See also Table S6.

of HF-SC quiescence (e.g., *Nfatc1* and *Fgf18*) (Figure 6B′, Figure S3A; Table S7A). Although the overall level of H3K27me3 modification over these genes was weak, this is probably reflective of the fact that only a fraction of the HF-SC population becomes activated during anagen (Hsu et al., 2011).

Interestingly, more HF-TAC signature genes gained the H3K79me2 mark in aHF-SCs than in qHF-SCs (42% versus 29%; Figure 6A′; Table S7B). Many of these appeared to be non-PcG-regulated cell cycle genes (Figure S3A′). Comparing all three populations, a hierarchy in cell cycle gene transcription and in mRNAs emerged: HF-TACs > aHF-SCs > qHF-SCs (Figure 6C, Figure S3B). In contrast to cell cycle genes, H3K27me3-marked key HF-TAC regulators remained PcG-repressed in aHF-SCs (Figure 6C′, Figure S3B). These results suggest that the qHF-SC to aHF-SC transition is controlled largely by transcripts changing from initiating to elongating states.

Because Wnt signaling/β-catenin stabilization is associated with anagen onset and transgenic mice that express elevated stabilized β-catenin (ΔN-βcat) display a shortened telogen, we examined whether elevated β-catenin signaling in qHF-SCs is sufficient to derepress PcG-marked key HF-TAC genes that are essential for the cell fact switch. To test this possibility, we performed ChIP-qPCR on key matrix regulator genes (Figure S4A). In agreement with their mRNA expression pattern (Figure S4B), key matrix regulator genes remained repressed while cell cycle genes, frequently upregulated during SC activation, remained unmarked by H3K27me3 in ΔN-βcat(+) qHF-SCs (Figure S4A). These data suggest that stabilization of β-catenin promotes transcription of a number of non-PcG-regulated cell cycle genes involved in the process of HF-SC activation. The bar for switching PcG-regulated fate determiners may require more robust signaling and/or additional pathways. The model in Figure 6D summarizes our findings on histone modification aspects in HF-SC activation and the TAC fate switch.

Loss of H3K27 Trimethylation Elicits Early Transcriptional Changes that Precede Phenotypic Signs of Flipping the PcG-Mediated HF Fate Switch

Previously, we conditionally targeted mice *Ezh1/2* resulting in a lack of H3K27me3 in the skin epithelium of P0 mice (Ezhkova et al., 2011). Although HFs had developed in these mice and no phenotypic signs of a fate-switch defect had been observed, this issue merited revisiting now that we had identified the key fate-switch genes that are PcG-regulated. To do so, we conducted mRNA profiling and qPCR analyses of purified populations of *Ezh1/2* null versus WT ORS/bulge and matrix. Intriguingly, in the absence of Ezh1/2, mRNAs expressed by key matrix genes were significantly upregulated in ORS/bulge, and conversely key HF-SC regulators failed to completely shut off in matrix (Figure S5A). That said, aberrant expression of these key PcG-regulated genes occurred at markedly lower levels than in the natural HF-SC to HF-TAC switch (Figure S5B). These results are reminiscent of those obtained previously with

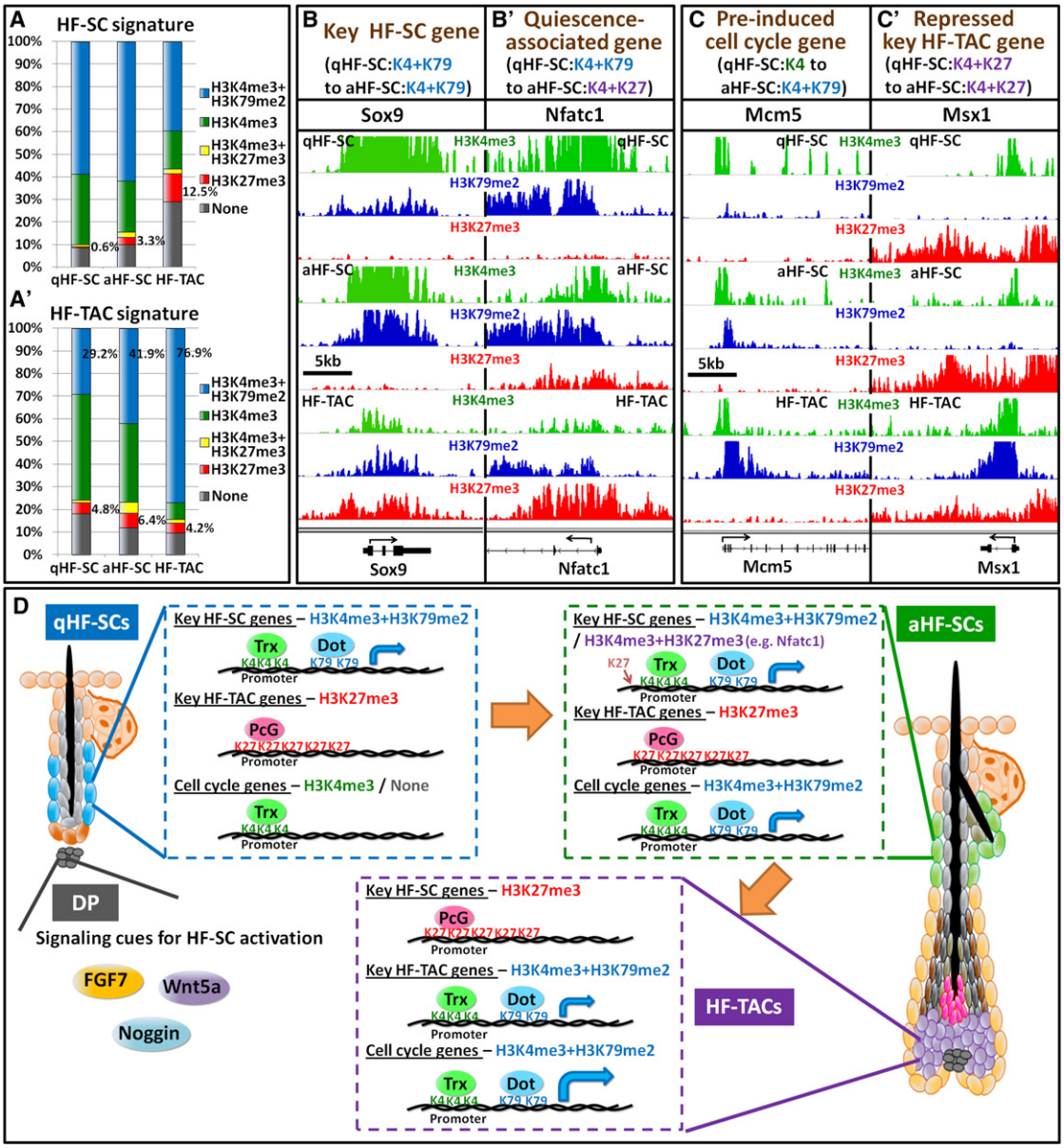

Figure 6. The Transition from Quiescent to Activated HF-SCs Maintains the Status of Many PcG-Regulated Genes, whereas Activating Cell Cycle Genes Are Not Governed by PcG

(A and A′) Chromatin characteristics of HF-SC (A) and HF-TAC (A′) signature genes are similar for quiescent and activated HF-SCs but distinct from HF-TACs.

(B and B′) Quiescent and activated HF-SC ChIP-seq profiles of key regulators of HF-SC maintenance (B) and quiescence (B′). All tracks are set to the same scale. Note chromatin changes in SC quiescence but not maintenance genes.

(C and C′) Cell cycle genes (e.g., *Mcm5* in C), but not key matrix regulators (e.g., *Msx1* in C′) are pre-induced in aHF-SCs. ChIP-seq profiles from quiescent and activated HF-SC and HF-TAC chromatin are shown.

(D) Working model for PcG-mediated regulation in governing an irreversible fate switch. In qHF-SCs, key HF-TAC genes are PcG-repressed, whereas HF-SC genes are PcG-free and actively transcribed. Upon activation, HF-SCs maintain SC characteristics, whereas a few genes associated with quiescence (e.g., *Fgf18*, *Nfatc1*) become repressed by PcG. In response to activating cues, aHF-SCs pre-induce (+H3K79me2) cell cycle genes that are not targeted by PcG; this induction is later enhanced upon transition to HF-TACs. Notably, HF-TAC regulators remain PcG-repressed in aHF-SCs, and this repression is not relieved until the HF fate is determined in TACs. Along with this derepression, HF-SC genes are now silenced by PcG in TA progeny. See also Figures S3, S4, and S5 and Table S7.

PcG-regulated nonskin genes (Ezhkova et al., 2011). Most importantly, however, they show that like Wnt activation, H3K27me3 loss is necessary but not sufficient to flip the powerful switch that sets the high threshold in HF-SCs for TAC fate commitment.

Exploiting Histone Modifications to Uncover New Insights into the Balance between Quiescence and Activation in the HF Stem Cell Niche

Our findings led us to wonder whether our knowledge of histone modification patterns might be used to facilitate the

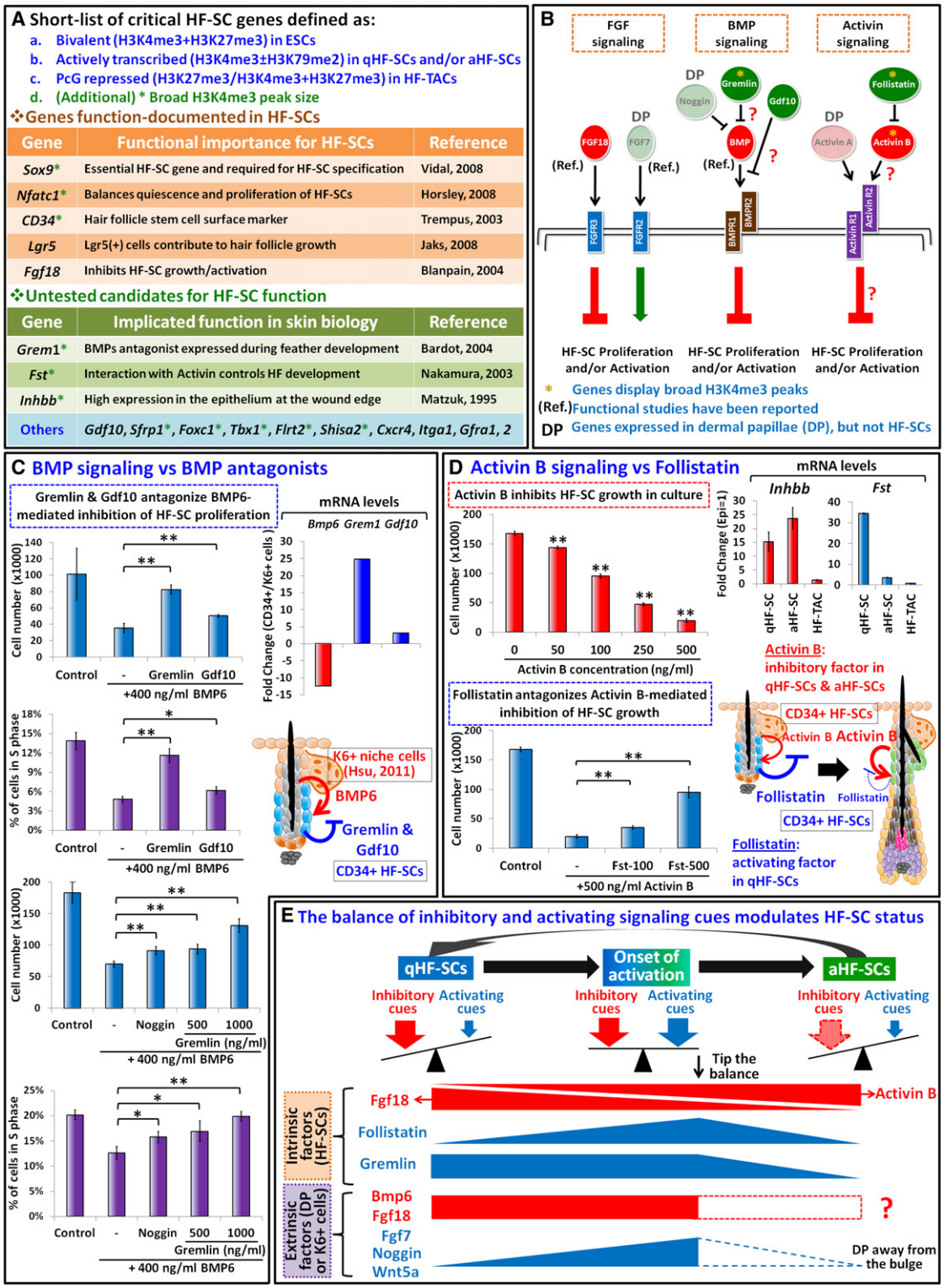

Figure 7. PcG-Regulated Signaling Pathways Mediate the Balance of HF-SC Quiescence and Activation

(A) HF-SC genes which share the listed chromatin/expression criteria are enriched for functionally important genes in HF-SCs (orange) and/or skin (green). A number of these genes encode signaling pathway factors or TFs of undetermined function in the skin/HF-SCs (blue). * Denotes genes exhibiting broad H3K4me3 peaks in qHF-SCs. (B) HF-SC signaling pathways from (A) that are predicted to impact proliferation and/or activation in a cell-autonomous fashion based solely upon the chromatin and transcriptional characteristics of their receptors and ligands. Ligands and antagonists for HF-SC receptors are expressed in HF-SCs (bright color) or DP (dim color). Anticipated proliferative effects of factors on HF-SCs are stimulatory (green) or inhibitory (red). (C) (Left) Recombinant Gremlin and

identification of key HF-SC regulators. We posited that these genes should be enriched in the subset that are (1) bivalent in ESCs; (2) actively transcribed in HF-SCs; (3) PcG-repressed in HF-TACs; and in some cases, (4) marked by a broad H3K4me3 peak. Interestingly, this increasingly shorter list still contained several TFs (*Sox9*, *Nfatc1*), transmembrane proteins (*Cd34*, *Lgr5*), and regulatory growth factors (*Fgf18*), already linked to HF-SC behavior (Figure 7A; Blanpain et al., 2004; Horsley et al., 2008; Jaks et al., 2008; Trempus et al., 2003; Vidal et al., 2005). Most notable was the persistence of several signaling genes, which, although functionally untested in HF-SCs, are predicted to function in BMP and Activin pathways (Bardot et al., 2004; Matzuk et al., 1995; Nakamura et al., 2003).

A scan of histone modification and mRNA profiles indicated that the surface receptor genes for FGF, BMP, and Activin pathways are all actively transcribed in both quiescent and activated HF-SCs (data not shown). Figure 7B summarizes their corresponding ligands identified from our short list and indicates how we posit they might be involved in HF-SCs based upon what is known (Blanpain and Fuchs, 2009; Greco et al., 2009; Hsu et al., 2011).

We first focused on *Grem1* and *Gdf10*, encoding putative BMP inhibitory factors. HF-SCs in vitro are growth-restricted when exposed to 400 ng/ml BMP6 (Blanpain et al., 2004). Interestingly, BMP6-mediated HF-SC growth inhibition was significantly ameliorated by coexposure to either growth factor, with Gremlin having the most potent effect (Figure 7C). The counteracting effects of these factors were reflected in the restoration of HF-SC cycling, as measured by 1 hr exposure to the nucleotide analog EdU prior to harvesting. Moreover, the antagonizing effects of Gremlin on BMP6 signaling were dose dependent (Figure 7C). Because both *Grem1* and *Gdf10* genes are PcG-repressed after HF-SCs transition to the activated state (Figure S6A), we speculate that these cell autonomous, BMP-inhibitory factors might function with DP-expressed Noggin to eventually override the high BMP6 levels imposed by the K6 inner bulge cells (Hsu et al., 2011) and activate HF-SCs (see Figure 7C).

Previously, it was reported that Activin antagonist Follistatin is expressed by human HF-SCs (Ohyama et al., 2006) and Activin in vivo functions in hair cycling (Qiu et al., 2011). Intriguingly, *Inhbb* encoding Activin B (activinβB-activinβB), and *Fst* encoding Follistatin (Figure 7B), were both marked by H3K79me2 and also displayed broad H3K4me3 peaks throughout the transition from HF-SC quiescence to activation (Figure S6B). Thus, we next focused on the possible relevance of this pathway.

Recombinant Activin B had a potent inhibitory effect, significantly reducing HF-SC proliferation in vitro in a dose-dependent fashion (Figure 7D, Figure S7A). At 500 ng/ml, 90% of HF-SC growth was restricted, an effect that was significantly counterbalanced by Follistatin in a dose-dependent fashion (Figure 7D, Figure S7B). Interestingly, Follistatin is also known to interfere with BMP signaling, albeit with lower affinity/potency. These data provide new insights into why *Fst* null embryos show retarded HF development (Nakamura et al., 2003) and suggest that its stimulatory effects may be required in adult mice to overcome the intrinsic inhibitory effects of Activin B signaling in HF-SCs (Figure 7D).

DISCUSSION

Cell Type versus Lineage Fate Switches

By monitoring chromatin marks in an adult SC population through stages of quiescence, activation, and lineage commitment, we discovered that in contrast to ESCs, only a small number of genes are bivalently marked by both H3K27me3 and H3K4me3. On the basis of similar in vitro findings on cultured neural cells differentiated from ESCs, our data suggest that bivalency may no longer be needed once tissue lineages have been selected and cell type options have been restricted.

Despite minimal signs of bivalency, PcG-mediated repression and derepression featured prominently in HF-SC and lineage genomes. As expected from prior studies made on individual genes, our global analyses showed that nonskin lineage master transcriptional regulators are uniformly silenced by H3K27me3 in the HF lineage. More interesting and unexpected were the select group of regulators involved in HF-SC lineage progression that were marked by H3K27me3. Some of these genes—the matrix regulators—remained PcG-repressed in both quiescent and active HF-SCs and were only derepressed in HF-TACs. Others—the HF-SC maintenance genes—remained active in HF-SCs and were only repressed in HF-TACs. Taken together, these findings unveil PcG-mediated repression/derepression as a double-edged sword in the lineage commitment switch from stemness to differentiation. Moreover, the congruent timing of these events suggests that the mechanism for repression and derepression is integrally linked.

It was also intriguing that many of the PcG-regulated genes in the HF lineage existed in a bivalent state in ESCs. On the basis of these findings, it could be that the foundations for the PcG switch are established during early embryogenesis and then modified during development to suit the tissue-specific needs of adult SCs. This finding is interesting in light of recent studies on

Gdf10 antagonize BMP6-mediated inhibition of HF-SC growth and proliferation in culture. HF-SCs were cultured for 5 days in the presence of 400 ng/ml BMP6 ± 1 μg/ml Gremlin or Gdf10. Control: Cells treated with vehicle. S phase cells were detected by EdU-pulse labeling. Data are reported as average ± SD; $^{**}p < 0.01$; $^{*}p < 0.05$. (Right) Relative fold changes in *Bmp6*, *Grem1*, *and Gdf10* mRNAs from $CD34^{+}$ HF-SCs and K6+ niche cells (unpublished microarray data, Hsu and Fuchs). Working model shows how proteins encoded by increased HF-SC *Gremlin* and *Gdf10* mRNA levels might antagonize BMP6-mediated inhibitory cues from K6+ niche cells (Hsu et al., 2011).

(D) As shown on the left, recombinant Activin B and Follistatin exert opposing effects on HF-SC proliferation in vitro. HF-SCs were cultured with indicated amounts of Activin B (top), and in the presence of 500 ng/ml Activin B, cells were treated ± 100 (Fst-100) or 500 ng/ml (Fst-500) Follistatin (bottom). Data are reported as average ± SD; $^{**}p < 0.01$; $^{*}p < 0.05$. As shown on the right, mRNA patterns of Activin B (*Inhbb*) and Follistatin (*Fst*). Model summarizes the results.

(E) Model summarizing how the balance of intrinsic/extrinsic inhibitory and activating signaling cues modulates HF-SC status. Prior studies concentrated on the influence of inhibitory and activating cues from the SC microenvironment. The short list of genes in (A) guided us to intrinsic regulators which we show contribute to this balancing act. See also Figures S6 and S7.

epigenetic reprogramming of induced pluripotent SCs, where H3K27me3 marks remained largely unchanged in the face of thousands of changes in H3K4me2 (Koche et al., 2011).

From Histone Methylation to Gene Expression to Functional Significance

In recent years, it has become increasingly clear that RNA polymerase II occupancy of the transcription initiation site and the accompanying H3K4me3 chromatin modification is necessary but not sufficient to dictate transcription and that "mediator" complexes associate with pausing factors to control elongation (Conaway and Conaway, 2011; Kagey et al., 2010). Although reliable measures of transcriptional elongation, such as H3K79me2 and H3K36me3, are now available (Vakoc et al., 2006), chromatin modifiers have been less optimal in gauging a gene's relative level of expression, even with the recent addition of so-called "chromatin readers" that fine-tune chromatin surrounding modified histone marks (Vermeulen et al., 2010).

Although the use of chromatin modifications as a blueprint for determining transcript levels is still in its early stages, we gained several new insights by comparing relative mRNA levels with associated chromatin modifications as HF-SCs transition through dormant and proliferative states and finally lineage commitment. Most notably, a gene more highly transcribed at one time within the lineage often displayed a broader H3K4me3 peak accompanied by stronger H3K79me2 marks throughout the body of the gene than when at a stage where its expression was lower. Possibly relevant to our findings are those on *Arabidopsis*, in which highly dense and narrow distributions of H3K4me3 near transcriptional start sites were associated with constitutive expression of genes involved in translation, while broad distributions toward coding regions correlated with expression of genes involved in key plant processes e.g., photosynthesis (Ha et al., 2011).

Indeed our data revealed that by screening the genes in our HF-SC signature first for bivalency in ESCs, then for H3K79me2-marked transcriptional elongation, often with a broad H3K4me3 peak, and finally for PcG repression in TACs, a short list of candidates sharing these histone modification criteria could be generated that was highly enriched for established HF-SC regulators. We exploited these data by functionally testing several signaling pathway genes on this short list. We focused on candidates whose corresponding surface receptor genes also showed H3K4me3 and H3K79me2 marks, suggesting that they could be cell-autonomous regulators of HF-SCs. Although further studies will be necessary to fully understand the roles of these signaling pathway members in HF-SC biology, our functional assays were sufficient to illustrate the power of using histone modification patterns as a blueprint for honing in on the key gene expression changes that occur as HF-SCs embark upon lineage commitment. Placed in context with the current literature, our results suggest a newfound complexity in the checks and balances imposed by intrinsic and extrinsic factors and signaling pathways on the HF-SC niche (Figure 7E).

The Role of PcG-Mediated Repression/Derepression in Lineage Commitment and Cell Fate Determination

The relative paucity of PcG-mediated changes in transitioning from quiescent to activated HF-SCs was as dramatic as the switch in PcG-repressed/relieved genes upon transition from HF-SCs to TA progeny. Additionally remarkable was the considerable threshold to PcG-mediated change that persisted in the face of enhanced stabilized β-catenin in HF-SCs. Indeed, although telogen HF-SCs exhibited transcriptional changes and increased proliferation in response to elevated β-catenin, the affected cell cycle genes did not seem to be ones marked by H3K27me3. By contrast, PcG-regulated cell fate commitment genes remained largely silent in HF-SCs.

Our findings suggest the following mechanistic framework: by utilizing transient and/or low Wnt/β-catenin to activate cell-cycle genes that are predominantly free of PcG-mediated control, HF-SCs can transition between quiescence and self-renewal while maintaining their undifferentiated state. By utilizing PcG modifications to regulate critical cell fate commitment genes, activated HF-SCs then must undergo a second step to overcome this threshold and transition to a point of no return. Finally, the PcG gatekeeper in this key decision is a two-way switch, reinforcing the likelihood that it will be irreversible.

How is this switch in PcG-target genes achieved during lineage commitment? Elevating the levels of stabilized β-catenin does not seem to be sufficient, nor does relieving PcG modification by loss of the H3K27 methylases Ezh1 and Ezh2. However, we know that during the normal hair cycle, the switch happens at the base of the mature HF, when prolonged interactions occur between DP and matrix. Taken together, our findings show that additional and/or elevated signals arising from this sustained crosstalk are likely to contribute with Wnts to elicit the SC→TAC transition. By placing a strong PcG-regulatory switch at cellular signaling crossroads, the commitment step involving key regulatory TFs becomes distinguished from the events that merely control HF-SC proliferation and don't change fate.

The requirements for multiple signaling inputs and transcriptional effectors in the switch mechanism provides us with a clearer understanding of why loss of PcG H3K27me3 modifications in the HF did not result in massive rapid activation of PcG-regulated genes, nor did it appear to cause a phenotypic fate switch in the HF-SC or matrix compartments (Ezhkova et al., 2011). Moreover, although HF-SC and matrix TAC proliferation were severely crippled by a marked deregulation of the PcG-regulated *Ink4a/Ink4b/Arf* locus upon *Ezh1/2* loss of function (Ezhkova et al., 2011), we found that changes in the *Ink4a/Ink4b/Arf* locus do not come into play during either normal HF-SC activation or lineage progression. Moreover, most cell cycle genes transcribed upon Wnt-mediated activation of HF-SCs and further upregulated during the transition to HF-TACs, did not appear to be under PcG control.

In closing, our findings show that adult SCs in the HF become active and self-renew by mechanisms that appear to involve mostly non-PcG regulated genes and a bimodal switch involving PcG-regulation is critical to control fate determination and lineage progression. In normal homeostasis, this rheostat does not trigger until multiple signaling inputs converge on the activated HF-SCs, unveiling a requirement for both transcriptional effectors and histone modifications in governing the complex processes of tissue homeostasis and regeneration.

EXPERIMENTAL PROCEDURES

Mice

Mice were housed in the AAALAC accredited Comparative Bioscience Center (CBC) at The Rockefeller University in accordance with NIH guidelines.

ChIP-seq Assay

All materials and methods for ChIP-seq have been described (Lee et al., 2006; Novershtern et al., 2011). Independent immunoprecipitations were performed on FACS-sorted populations from female mice. A total of 3 × 10^6 cells were used for each ChIP-seq run. Sorted cells were crosslinked by addition of 1/10th volume of fresh 11% formaldehyde solution for 10 min (min.) at room temperature (r.t.) and then rinsed twice with 1× phospho-buffered saline (PBS) prior to freezing in liquid nitrogen and storing at –80°C. Before ChIP, cells were resuspended, lysed, and sonicated to solubilize and shear crosslinked DNAs. For sonication, lysates were treated with Triton X-100 to 1% and then subjected to a Bioruptor Sonicator (Diagenode, UCD-200) according to a 30× regiment of 30 s (sec.) sonication followed by 60 s rest. The resulting whole-cell extract was incubated overnight at 4°C with 10 μl of Dynal Protein G magnetic beads (Invitrogen), which had been preincubated with ~5 μg of the appropriate Ab. After ChIP, samples were washed with low salt, high salt, LiCl, and Tris-EDTA buffer for 5 min. Bound complexes were eluted and crosslinking was reversed by overnight (o/n) incubation at 65°C. Whole-cell extract DNA was also treated for crosslink reversal.

ChIP-Seq Sample Preparation and Analysis

ChIP DNA was prepared for sequencing (Novershtern et al., 2011) with a few modifications. In brief, a single adenine nucleotide overhang was added to the fragmented DNAs to allow for directional ligation. A 1:500 dilution of the Adaptor Oligo Mix (Illumina) was used in the ligation step. A subsequent PCR step with 25 amplification cycles added the additional Solexa linker sequence to the fragments to prepare them for annealing to the Genome Analyzer flow cell. After amplification, a narrow range of fragment sizes was selected by separation on a 2% agarose gel and excision of a band between 150 and 300 bp. The DNA was purified from the agarose and diluted to 10 nM for loading on the flow cell. Sequencing was performed on an Illumina/Solexa Genome Analyzer 2 in accordance with the manufacturer's protocols.

ChIP-Seq reads were aligned to the mouse genome (mm9, build 37) with the Bowtie program (Langmead et al., 2009) and the Illumina Analyzer Pipeline. Unique reads mapped to a single genomic location (allowing two mismatches) were kept for peak identification with the software MACS (Zhang et al., 2008). Sequencing reads from input DNA were used as control for MACS. Peak heights were subsequently computed with in-house software and used to filter out false positive peaks of low signal intensities. Annotated mouse RefSeq genes with a peak at their promoters (−2 kb to +2 kb of transcription start sites) were then considered as targets of K4, K27, or K79 modifications. Genes without a modification mark in any of our cell types were excluded in our statistics. To compute the level of a histone modification, we summed the total of ChIP-Seq reads mapped to individual promoters and this total was then normalized with sequencing depth to obtain comparable data across cell types. To identify genes with large H3K4me3 peaks in qHF-SCs, we utilized the peak sizes from MACS and selected for peaks that were >4 kb and whose sizes were >3X larger in qHF-SCs than in matrix cells (or no peak identified in matrix cells).

ACCESSION NUMBERS

Microarray and ChIP-seq data have been submitted to NCBI-GEO under accession numbers GSE31028 and GSE31239, respectively.

SUPPLEMENTAL INFORMATION

Supplemental Information includes seven figures, seven tables, and Supplemental Experimental Procedures and can be found with this article online at doi:10.1016/j.stem.2011.07.015.

ACKNOWLEDGMENTS

We thank S. Dewell for assistance in high-throughput sequencing and analysis (RU Genomics Resource Center); A. Viale, D. You, and J. Zhao for microarray (MSKCC microarray facility); S. Mazel, L. Li, A. Lloyd, and S. Tadesse for FACS sorting (RU FACS facility); and K.-M. Noh (Allis lab, RU) for providing ESC cDNAs. We also thank Fuchs' lab members N. Stokes and D. Oristian for assistance in mouse research (Fuchs lab); E. Ezhkova for *Ezh1/2* dKO cDNA samples; Y.-C. Hsu for unpublished microarray information; and A. Folgueras, E. Ezhkova, L. Zhang, S. Beronja, B. Keyes, M. Kadaja, Y.-C. Hsu, and T. Chen for discussions and comments on the manuscript. W.-H.L. was supported by a Harvey L. Karp Postdoctoral Fellowship and is currently a Jane Coffin Child Postdoctoral Fellow. E.F. is an HHMI Investigator. This work was supported by a grant (to E.F.) from the NIH/NIAMS (R01AR31737) and partially by NIH/NIMH (R21MH087840, D.Z.).

Received: March 4, 2011
Revised: July 4, 2011
Accepted: July 28, 2011
Published: September 1, 2011

REFERENCES

Adli, M., Zhu, J., and Bernstein, B.E. (2010). Genome-wide chromatin maps derived from limited numbers of hematopoietic progenitors. Nat. Methods *7*, 615–618.

Bardot, B., Lecoin, L., Fliniaux, I., Huillard, E., Marx, M., and Viallet, J.P. (2004). Drm/Gremlin, a BMP antagonist, defines the interbud region during feather development. Int. J. Dev. Biol. *48*, 149–156.

Barski, A., Cuddapah, S., Cui, K., Roh, T.Y., Schones, D.E., Wang, Z., Wei, G., Chepelev, I., and Zhao, K. (2007). High-resolution profiling of histone methylations in the human genome. Cell *129*, 823–837.

Bernstein, B.E., Mikkelsen, T.S., Xie, X., Kamal, M., Huebert, D.J., Cuff, J., Fry, B., Meissner, A., Wernig, M., Plath, K., et al. (2006). A bivalent chromatin structure marks key developmental genes in embryonic stem cells. Cell *125*, 315–326.

Blanpain, C., and Fuchs, E. (2009). Epidermal homeostasis: A balancing act of stem cells in the skin. Nat. Rev. Mol. Cell Biol. *10*, 207–217.

Blanpain, C., Lowry, W.E., Geoghegan, A., Polak, L., and Fuchs, E. (2004). Self-renewal, multipotency, and the existence of two cell populations within an epithelial stem cell niche. Cell *118*, 635–648.

Boyer, L.A., Lee, T.I., Cole, M.F., Johnstone, S.E., Levine, S.S., Zucker, J.P., Guenther, M.G., Kumar, R.M., Murray, H.L., Jenner, R.G., et al. (2005). Core transcriptional regulatory circuitry in human embryonic stem cells. Cell *122*, 947–956.

Boyer, L.A., Plath, K., Zeitlinger, J., Brambrink, T., Medeiros, L.A., Lee, T.I., Levine, S.S., Wernig, M., Tajonar, A., Ray, M.K., et al. (2006). Polycomb complexes repress developmental regulators in murine embryonic stem cells. Nature *441*, 349–353.

Chen, H., Gu, X., Su, I.H., Bottino, R., Contreras, J.L., Tarakhovsky, A., and Kim, S.K. (2009). Polycomb protein Ezh2 regulates pancreatic beta-cell Ink4a/Arf expression and regeneration in diabetes mellitus. Genes Dev. *23*, 975–985.

Cole, M.F., Johnstone, S.E., Newman, J.J., Kagey, M.H., and Young, R.A. (2008). Tcf3 is an integral component of the core regulatory circuitry of embryonic stem cells. Genes Dev. *22*, 746–755.

Conaway, R.C., and Conaway, J.W. (2011). Function and regulation of the Mediator complex. Curr. Opin. Genet. Dev. *21*, 225–230.

Cotsarelis, G., Sun, T.T., and Lavker, R.M. (1990). Label-retaining cells reside in the bulge area of pilosebaceous unit: Implications for follicular stem cells, hair cycle, and skin carcinogenesis. Cell *61*, 1329–1337.

Ezhkova, E., Pasolli, H.A., Parker, J.S., Stokes, N., Su, I.H., Hannon, G., Tarakhovsky, A., and Fuchs, E. (2009). Ezh2 orchestrates gene expression for the stepwise differentiation of tissue-specific stem cells. Cell *136*, 1122–1135.

Ezhkova, E., Lien, W.H., Stokes, N., Pasolli, H.A., Silva, J.M., and Fuchs, E. (2011). EZH1 and EZH2 cogovern histone H3K27 trimethylation and are essential for hair follicle homeostasis and wound repair. Genes Dev. *25*, 485–498.

Fuchs, E. (2007). Scratching the surface of skin development. Nature *445*, 834–842.

Greco, V., Chen, T., Rendl, M., Schober, M., Pasolli, H.A., Stokes, N., Dela Cruz-Racelis, J., and Fuchs, E. (2009). A two-step mechanism for stem cell activation during hair regeneration. Cell Stem Cell *4*, 155–169.

Ha, M., Ng, D.W., Li, W.H., and Chen, Z.J. (2011). Coordinated histone modifications are associated with gene expression variation within and between species. Genome Res. *21*, 590–598.

Horsley, V., Aliprantis, A.O., Polak, L., Glimcher, L.H., and Fuchs, E. (2008). NFATc1 balances quiescence and proliferation of skin stem cells. Cell *132*, 299–310.

Hsu, Y.C., Pasolli, H.A., and Fuchs, E. (2011). Dynamics between stem cells, niche, and progeny in the hair follicle. Cell *144*, 92–105.

Jaks, V., Barker, N., Kasper, M., van Es, J.H., Snippert, H.J., Clevers, H., and Toftgård, R. (2008). Lgr5 marks cycling, yet long-lived, hair follicle stem cells. Nat. Genet. *40*, 1291–1299.

Kagey, M.H., Newman, J.J., Bilodeau, S., Zhan, Y., Orlando, D.A., van Berkum, N.L., Ebmeier, C.C., Goossens, J., Rahl, P.B., Levine, S.S., et al. (2010). Mediator and cohesin connect gene expression and chromatin architecture. Nature *467*, 430–435.

Kirmizis, A., Bartley, S.M., Kuzmichev, A., Margueron, R., Reinberg, D., Green, R., and Farnham, P.J. (2004). Silencing of human polycomb target genes is associated with methylation of histone H3 Lys 27. Genes Dev. *18*, 1592–1605.

Koche, R.P., Smith, Z.D., Adli, M., Gu, H., Ku, M., Gnirke, A., Bernstein, B.E., and Meissner, A. (2011). Reprogramming factor expression initiates widespread targeted chromatin remodeling. Cell Stem Cell *8*, 96–105.

Langmead, B., Trapnell, C., Pop, M., and Salzberg, S.L. (2009). Ultrafast and memory-efficient alignment of short DNA sequences to the human genome. Genome Biol. *10*, R25.

Lee, T.I., Jenner, R.G., Boyer, L.A., Guenther, M.G., Levine, S.S., Kumar, R.M., Chevalier, B., Johnstone, S.E., Cole, M.F., Isono, K., et al. (2006). Control of developmental regulators by Polycomb in human embryonic stem cells. Cell *125*, 301–313.

Li, B., Carey, M., and Workman, J.L. (2007). The role of chromatin during transcription. Cell *128*, 707–719.

Lowry, W.E., Blanpain, C., Nowak, J.A., Guasch, G., Lewis, L., and Fuchs, E. (2005). Defining the impact of beta-catenin/Tcf transactivation on epithelial stem cells. Genes Dev. *19*, 1596–1611.

Marson, A., Levine, S.S., Cole, M.F., Frampton, G.M., Brambrink, T., Johnstone, S., Guenther, M.G., Johnston, W.K., Wernig, M., Newman, J., et al. (2008). Connecting microRNA genes to the core transcriptional regulatory circuitry of embryonic stem cells. Cell *134*, 521–533.

Matzuk, M.M., Lu, N., Vogel, H., Sellheyer, K., Roop, D.R., and Bradley, A. (1995). Multiple defects and perinatal death in mice deficient in follistatin. Nature *374*, 360–363.

Mikkelsen, T.S., Ku, M., Jaffe, D.B., Issac, B., Lieberman, E., Giannoukos, G., Alvarez, P., Brockman, W., Kim, T.K., Koche, R.P., et al. (2007). Genome-wide maps of chromatin state in pluripotent and lineage-committed cells. Nature *448*, 553–560.

Nakamura, M., Matzuk, M.M., Gerstmayer, B., Bosio, A., Lauster, R., Miyachi, Y., Werner, S., and Paus, R. (2003). Control of pelage hair follicle development and cycling by complex interactions between follistatin and activin. FASEB J. *17*, 497–499.

Nguyen, H., Merrill, B.J., Polak, L., Nikolova, M., Rendl, M., Shaver, T.M., Pasolli, H.A., and Fuchs, E. (2009). Tcf3 and Tcf4 are essential for long-term homeostasis of skin epithelia. Nat. Genet. *41*, 1068–1075.

Novershtern, N., Subramanian, A., Lawton, L.N., Mak, R.H., Haining, W.N., McConkey, M.E., Habib, N., Yosed, N., Chang, C.Y., Shay, T., et al. (2011). Densely interconnected transcriptional circuits control cell states in human hematopoiesis. Cell *144*, 296–309.

Ohyama, M., Terunuma, A., Tock, C.L., Radonovich, M.F., Pise-Masison, C.A., Hopping, S.B., Brady, J.N., Udey, M.C., and Vogel, J.C. (2006). Characterization and isolation of stem cell-enriched human hair follicle bulge cells. J. Clin. Invest. *116*, 249–260.

Pokholok, D.K., Harbison, C.T., Levine, S., Cole, M., Hannett, N.M., Lee, T.I., Bell, G.W., Walker, K., Rolfe, P.A., Herbolsheimer, E., et al. (2005). Genome-wide map of nucleosome acetylation and methylation in yeast. Cell *122*, 517–527.

Qiu, W., Li, X., Tang, H., Huang, A.S., Panteleyev, A.A., Owens, D.M., and Su, G.H. (2011). Conditional activin receptor type 1B (Acvr1b) knockout mice reveal hair loss abnormality. J. Invest. Dermatol. *131*, 1067–1076.

Rendl, M., Lewis, L., and Fuchs, E. (2005). Molecular dissection of mesenchymal-epithelial interactions in the hair follicle. PLoS Biol. *3*, e331.

Su, I.H., Basavaraj, A., Krutchinsky, A.N., Hobert, O., Ullrich, A., Chait, B.T., and Tarakhovsky, A. (2003). Ezh2 controls B cell development through histone H3 methylation and Igh rearrangement. Nat. Immunol. *4*, 124–131.

Trempus, C.S., Morris, R.J., Bortner, C.D., Cotsarelis, G., Faircloth, R.S., Reece, J.M., and Tennant, R.W. (2003). Enrichment for living murine keratinocytes from the hair follicle bulge with the cell surface marker CD34. J. Invest. Dermatol. *120*, 501–511.

Vakoc, C.R., Sachdeva, M.M., Wang, H., and Blobel, G.A. (2006). Profile of histone lysine methylation across transcribed mammalian chromatin. Mol. Cell. Biol. *26*, 9185–9195.

Vermeulen, M., Eberl, H.C., Matarese, F., Marks, H., Denissov, S., Butter, F., Lee, K.K., Olsen, J.V., Hyman, A.A., Stunnenberg, H.G., and Mann, M. (2010). Quantitative interaction proteomics and genome-wide profiling of epigenetic histone marks and their readers. Cell *142*, 967–980.

Vidal, V.P., Chaboissier, M.C., Lützkendorf, S., Cotsarelis, G., Mill, P., Hui, C.C., Ortonne, N., Ortonne, J.P., and Schedl, A. (2005). Sox9 is essential for outer root sheath differentiation and the formation of the hair stem cell compartment. Curr. Biol. *15*, 1340–1351.

Zhang, Y., Liu, T., Meyer, C.A., Eeckhoute, J., Johnson, D.S., Bernstein, B.E., Nusbaum, C., Myers, R.M., Brown, M., Li, W., and Liu, X.S. (2008). Model-based analysis of ChIP-Seq (MACS). Genome Biol. *9*, R137.

Zhao, X.D., Han, X., Chew, J.L., Liu, J., Chiu, K.P., Choo, A., Orlov, Y.L., Sung, W.K., Shahab, A., Kuznetsov, V.A., et al. (2007). Whole-genome mapping of histone H3 Lys4 and 27 trimethylations reveals distinct genomic compartments in human embryonic stem cells. Cell Stem Cell *1*, 286–298.